ACCSCIENCE PUBLISHING

International Journal of Bioprinting

RESEARCH ARTICLE

A visible light-crosslinkable decellularized kidney matrix bioink for 3D bioprinting of organoids and drug testing

Wenqi Hu[1,2†], Guohua Wu[3], Mengjiao Xia[6], Di Wu[4,5], Qijun Du[1,2,6], Qinrui Lu[1,2], Jiashu Wang[1,2], Ao Xie[1,2], Chenwei Sun[1,2], Haijie Hu[7], Litian Zhao[1,2], Zipeng Yao[1,2,6†*], and Shuqi Wang[1,2,6,8]

[1]College of Biomedical Engineering, Sichuan University, Chengdu, Sichuan, China

[2]National Engineering Research Center for Biomaterials, Sichuan University, Chengdu, Sichuan, China

[3]Luoyang Key Laboratory of Clinical Multiomics and Translational Medicine, Henan Key Laboratory of Rare Diseases, Endocrinology and Metabolism Center, The First Affiliated Hospital and College of Clinical Medicine, Henan University of Science and Technology, Luoyang, Henan, China

[4]Henan Key Laboratory of Rare Diseases, Endocrinology and Metabolism Center, The First Affiliated Hospital and College of Clinical Medicine, Henan University of Science and Technology, Luoyang, Henan, China

[5]Department of Respiratory and Critical Care Medicine, West China Hospital, Sichuan University, Chengdu, Sichuan, China

[6]State Key Laboratory of Respiratory Health and Multimorbidity, West China Hospital, Sichuan University, Chengdu, Sichuan, China

[7]Division of Biliary Surgery, Department of General Surgery, West China Hospital, Sichuan University, Chengdu, Sichuan, China

[8]Clinical Research Center for Respiratory Disease, West China Hospital, Sichuan University, Chengdu, Sichuan, China

[†]These authors contributed equally to this work.

***Corresponding author:**
Zipeng Yao
(yetiman@163.com)

Citation: Hu W, Wu G, Xia M, *et al*. A visible light-crosslinkable decellularized kidney matrix bioink for 3D bioprinting of organoids and drug testing. *Int J Bioprint*. 2026;12(1):432-447. doi: 10.36922/IJB025480497

Received: November 27, 2025
Revised: December 11, 2025
Accepted: December 15, 2025
Published online: December 19, 2025

Abstract

Decellularized kidney extracellular matrix (DKM) is an acellular scaffold rich in structural proteins and glycosaminoglycans that can promote tissue regeneration and support organoid culture. Porcine-derived DKM contains abundant extracellular matrix (ECM) components, such as collagen, laminin, and fibronectin, and offers native biochemical cues. However, conventional decellularized ECM hydrogels often exhibit weak mechanical properties, poor printability, and slow gelation, limiting their use in high-throughput applications. Here, we report a visible-light-mediated crosslinking strategy for rapid gelation of DKM based on a tris(2,2′-bipyridyl) ruthenium (II) chloride hexahydrate/sodium persulfate (Ru/SPS) photoinitiator system. Illumination at 405 nm (30 mW/cm^2) in the presence of Ru/SPS achieves gelation in about 40 s, yielding a composite DKM–Ru/SPS bioink with tunable modulus by adjusting DKM, Ru, and SPS concentrations. High-fidelity 3D constructs were produced by extrusion bioprinting using a representative formulation (15 mg/mL DKM, 0.25 mM Ru, 2.5 mM SPS). As proof of concept, organoids encapsulated in the DKM–Ru/SPS bioink exhibited viability, proliferation, and lineage marker expression during culture. This work demonstrates a rapid, cell-compatible photocrosslinking approach for DKM–Ru/SPS that integrates organoid culture with 3D bioprinting and drug testing, supporting its potential use as a standardized bioink in tissue engineering and functional screening.

Keywords: 3D bioprinting; Decellularized kidney matrix; Drug screening; Organoid culture; Visible-light-crosslinkable

1. Introduction

Out of every 10 drug candidates undergoing clinical trials, only one typically receives Food and Drug Administration (FDA) approval, primarily due to unforeseen toxicity. Traditional methodologies, such as two-dimensional (2D) cell cultures and animal models, are insufficient in this regard: 2D cultures fail to replicate the complexity of human biology, while animal models are hindered by interspecies differences, low throughput, high costs, lengthy processes, and ethical concerns, all of which diminish their predictive accuracy for human outcomes.[1] In response to this challenge, three-dimensional (3D) organoid models have been established. Organoids derived from various stem cell sources harness the intrinsic self-organizing capacity of stem cells to form multicellular structures that closely mimic the architecture, functionality, and cellular heterogeneity of human organs.[2–4] Because organoids retain the morphology and genetic features of the source tissues, their reactions to external stimuli, including pharmacological agents, closely resemble those of native tissues, thereby improving the reliability of drug evaluation.[5–7]

The establishment and growth of these 3D structures critically depend on an embedding hydrogel matrix, which provides indispensable structural support and biochemical cues. Matrigel, derived from Engelbreth–Holm–Swarm mouse sarcoma, is widely recognized as the standard substrate for organoid culture.[8] However, its inherent limitations hinder advancements in precision oncology. Additionally, its origin from a nonhuman species poses challenges for clinical application. The low Young's modulus of Matrigel (<2 kPa) inadequately mimics the rigid, fibrotic stroma typical of advanced cancers, which plays a critical role in tumor progression and drug resistance.[9] Furthermore, Matrigel lacks the high collagen fiber content found in tumor tissues, potentially failing to accurately replicate the tumor microenvironment.[10–12]

Decellularized extracellular matrix (dECM) hydrogels offer a natural microenvironment for cell attachment and organoid development due to the absence of immunogenic cells and the presence of essential extracellular matrix (ECM) components.[13–17] Unlike synthetic hydrogels, tissue-specific dECM can increase the physiological relevance of organoids and improve translational fidelity. For example, decellularized kidney matrix (DKM) is rich in collagen IV and laminin, providing vital niche signals. However, DKM hydrogels often rely on thermoresponsive crosslinking, resulting in slow gelation (over 30 min) and temperature-dependent mechanical properties, making them unsuitable for automated high-throughput applications like 3D bioprinting, which is essential for addressing variability and standardization challenges in manual organoid culture.[13,18] Therefore, it is essential to develop methods for producing dECM-based hydrogels with rapid gelation. Various ultraviolet-responsive hydrogels, such as methylcellulose–norbornene gelatin,[19] methacrylated gelatin,[20,21] and polyethylene glycol-based hydrogels,[22,23] can harm cells. In contrast, a visible light-activated tris(2,2'-bipyridyl) ruthenium (II) chloride hexahydrate/sodium persulfate (Ru/SPS) system enables dityrosine crosslinking in ECM proteins (e.g., collagen) without prior chemical modification, thereby allowing efficient visible-light crosslinking of DKM. Traditional organoid cultures struggle with high-throughput drug testing due to labor demands, scalability limitations, and standardization issues, leading to bias and variability.[24–26] In contrast, 3D bioprinting offers precise and reproducible organoid formation, overcoming drawbacks of manual methods, such as heterogeneity and labor intensity. It supports the generation of automated organoid arrays, which are ideal for high-throughput screening.[27–29] To date, no studies have explored DKM–Ru/SPS hydrogels for 3D bioprinted organoids or systematically examined dECM-derived photocrosslinkable bioinks, despite their potential to maintain bioactivity and customizable properties for cell and drug delivery.

In this study, we utilized visible light-mediated crosslinking to create a DKM–Ru/SPS hydrogel bioink. We analyzed the decellularized matrix and its light-crosslinking materials at various concentrations, focusing on properties like ECM preservation, endotoxin levels, microstructure, and rheological behavior. We assessed cytocompatibility and organoid growth in DKM–Ru/SPS compared with Matrigel, demonstrating its suitability for printed organoid arrays and drug treatment workflows. The bioink's viability for organoid culture was evaluated to determine the optimal formulation. Additionally, the DKM–Ru/SPS bioink was combined with organoids and processed using a 3D bioprinter for drug sensitivity testing. This study presents a workflow that integrates rapid photogelation with 3D bioprinting to overcome challenges associated with dECM hydrogels, such as slow gelation and poor printability, while preserving bioactivity. It lays

the foundation for standardized, scalable, and automated organoid culture and drug testing.

2. Materials and methods

2.1. Porcine tissue decellularization and DKM–Ru/SPS solution preparation

Porcine kidneys were collected from a local market and preserved at −80°C. Tissues underwent three freeze–thaw cycles, were thawed to room temperature, and were cut into 5 × 5 × 5 mm pieces to increase the surface contact area. The cut tissue pieces were flushed three times (30 min each) with sterile water containing 100 U/mL penicillin and 100 μg/mL streptomycin (P/S) until all visible blood traces were removed. The rinse steps were as follows: (i) 1% sodium dodecyl sulfate (SDS; ≥ 99.9%; Sigma-Aldrich, St Louis, MO) in sterile water for 24 h (exchanged at 12 h), (ii) sterile water for 6 h, (iii) 1% Triton X-100 (Sigma-Aldrich) in sterile water for 48–72 h (exchanged daily), (iv) sterile water for 12 h until no foam was observed, and (v) 60 U/mL DNase I for 2 h. Finally, the tissue pieces were rinsed with sterile water containing P/S. All steps were performed on a magnetic stirrer (200 rpm, 25°C), and all solutions were filtered. The decellularized pieces were lyophilized for 72 h, milled into powder (<1 mm), and preserved at −80°C.

Dry DKM powder (10 mg) was dissolved in 1 mL of 1 mg/mL pepsin (Sigma-Aldrich) in hydrochloric acid solution (0.1 M) and digested at 25°C for 72 h with constant stirring (200 rpm). Digestion was terminated by neutralizing the solution to pH 7.4 with 1 N NaOH in 10× phosphate-buffered saline (PBS) on ice. Subsequently, Ru/SPS powder was dissolved in the DKM solution (1 mL) under stirring to obtain the DKM–Ru/SPS bioink, which was stored at 4°C in the dark. To observe thermogelation, the DKM solution and Matrigel were placed at 37°C for varying durations. To validate photocrosslinking, the DKM–Ru/SPS bioink was exposed to 405 nm visible light for 40 s, and gelation was confirmed using the Eppendorf tilting method.

2.2. Characterization of decellularized tissues

To evaluate cellular removal, native and decellularized tissues were fixed with 4% paraformaldehyde overnight, embedded in optimal cutting temperature compound, frozen, and sectioned (4 μm). Tissue slides were stained with hematoxylin and eosin (H&E) and Masson's trichrome and observed under a Zeiss microscope (Oberkochen, Germany). DNA content was quantified to assess decellularization. DNA was extracted from 100 mg samples using a TIANAmp DNA kit (Tiangen, China) according to the manufacturer's protocol, and total DNA content was quantified using a Nanodrop spectrophotometer (NanoDrop Lite, Thermo Fisher Scientific, USA).

Sulfated glycosaminoglycan (GAG) and collagen contents in native and decellularized tissues were quantified using Blyscan GAGs and collagen assay kits (Biocolor, UK) following the manufacturer's instructions to assess ECM preservation. Endotoxin levels in dECM hydrogels were measured using a Limulus Amebocyte Lysate chromogenic quantitation kit (Meimian, China). Residual SDS was quantified using a detection kit (Sangon Biotech, China) according to the manufacturer's guidelines. Transforming growth factor-beta (TGF-β), insulin-like growth factor 1 (IGF-1), and epidermal growth factor (EGF) concentrations in the DKM solution were measured using enzyme-linked immunosorbent assay kits (Meimian, China), and optical density values (n = 3) were read at 450 nm. The microstructure of the dECM hydrogel was examined by scanning electron microscopy (SEM; SU5000, Hitachi, Japan). Hydrogels were fixed in 2% osmium tetroxide, washed, dehydrated through an ascending ethanol gradient, vacuum dried, and sputter-coated with gold.

2.3. Evaluation of rheological properties of DKM–Ru/SPS bioink

Rheological characteristics were evaluated using a rheometer (TA Instruments, USA) with a 15 mm plate. Storage (G') and loss (G'') moduli of DKM (10, 15, and 20 mg/mL) mixed with varying Ru/SPS concentrations (0.125, 0.25, and 0.5 mM) were determined via strain sweep (0.01–10% strain). Steady shear sweep analyses were conducted at 25°C to investigate shear-thinning properties. For stability analysis, DKM–Ru/SPS bioink droplets (5 mm diameter) were dispensed, submerged in PBS, and cultured at 37°C, while gel morphology, diameter, and area were monitored. All rheological measurements were performed in triplicate.

To characterize various DKM hydrogels and Matrigel, Young's modulus was assessed as an indicator of stiffness. The hydrogels were shaped into cylinders with a height of 3 mm and a diameter of 7 mm and cured in an incubator at 37°C or under 405 nm visible light. A mechanical analyzer (EFL-MT5600, Suzhou, China) was used to measure the Young's modulus of the hydrogels at a rate of 1 mm/min at room temperature. The maximum load was set to 1 N.

2.4. Compatibility of the DKM–Ru/SPS bioink material

L929 cells were cultured in medium supplemented with 15% fetal bovine serum and 0.5% P/S. Cells were maintained at 37°C and 5% carbon dioxide (CO_2), passaged at a 1:3 ratio at 90% confluence, and the medium was refreshed

every 2 days. For 3D culture, L929 cells were mixed into the ice-cold DKM–Ru/SPS bioink (10,000 cells/25 μL) and plated in a 48-well plate. After gelation, 500 μL of culture media was added to each well, and the encapsulated cells were incubated. Cell viability was assessed using a live/dead assay kit (Invitrogen, USA). A staining solution (3 μL calcein-acetoxymethyl ester and 2 μL PI in 1 mL PBS) was added (500 μL/well) and incubated for 30 min at 37°C. Cells were imaged at distinct time points using fluorescence microscopy (Propidium iodide, Zeiss). All experiments were performed in triplicate.

2.5. Organoid establishment and passage

Mouse lung and liver tissues were harvested according to protocols approved by the Institutional Animal Care and Use Committee of West China Hospital, Sichuan University (Approval No. 108, 2023). Adipose tissue was dissected, and tissues were rinsed with Dulbecco's PBS, minced, and enzymatically digested with type IV collagenase (1 mg/mL) and DNase I (0.1 mg/mL) in Dulbecco's Modified Eagle Medium (DMEM) GlutaMAX (Gibco, USA) at 37°C for 30 min. Digestion was stopped by adding DMEM GlutaMAX. The suspension was filtered through a 100 μm strainer, centrifuged (299 g, 5 min), and the pellet was treated with 1 mL red blood cell lysis buffer (Servicebio, China) for 15 min. After washing, the cell pellet was counted and embedded (5×10^4 cells/well) in 30 μL of Matrigel or DKM–Ru/SPS in a 24-well plate. Matrigel was cured for 30 min (37°C), while the DKM–Ru/SPS bioink was cured using 405 nm light. Organoid medium (Aimingtmed, China) supplemented with 0.1% Y-27632 was added. Organoid formation efficiency and size were quantified.

For passaging, Matrigel was degraded with TrypLE (37°C, 5 min), and the DKM–Ru/SPS bioink was degraded with 5 mg/mL collagenase I (37 °C, 10 min). Harvested organoids were rinsed and re-encapsulated. Organoids were passaged every 5–10 days. Viability was assessed using a live/dead assay kit (Invitrogen, USA) and imaged by fluorescence microscopy (Zeiss). For cryopreservation, collected organoids were centrifuged (299 g, 5 min) and resuspended in cryopreservation solution (Gibco). For immunohistochemistry, lung organoids were fixed with paraformaldehyde, permeabilized with 1% Triton X-100, and sections were incubated overnight with antibodies against thyroid transcription factor-1 (TTF-1, a marker of lung progenitor and alveolar epithelial cells) and p63 (a basal cell marker), or subjected to H&E staining.

2.6. Drug assay

After 7 days of culture, the culture medium was replaced with medium containing varying doses of sorafenib, cisplatin, and acetaminophen (1, 10, 25, and 50 μM) for cytotoxicity assessment in liver organoids. After drug treatment, representative images of live/dead staining cells were acquired at 72 h utilizing an inverted fluorescent microscope (Zeiss, Oberkochen, Germany) to examine morphological alterations.

2.7. 3D bioprinting

A 3D bioprinter was utilized to fabricate a droplet microarray, resulting in a homogeneously dispersed bioink array. By modulating the printing nozzle inner diameter, platform temperature, and extrusion pressure, the consistency of the printed droplet sphere diameters was evaluated. By validating the outcomes of various parameters, optimization of the printing conditions was achieved.

The bioprinter was further employed to fabricate organoid arrays. Using software programming, dispense positions for a 12 × 8 array were designed as coordinates. The bioprinter nozzle was installed on the platform, and bioink was extruded at a specified pressure. This printing method was utilized to fabricate organoid arrays. Once printing and curing were completed, organoid medium was introduced, and the constructs were maintained in an incubator at 37 °C with 5% CO_2. The bioink was printed using a 3D bioprinter in a 96-well plate to obtain designed patterns to evaluate the consistency and reliability of the 3D system.

Organoid models were generated using the designed 3D bioprinting system. A syringe was loaded with DKM–Ru/SPS bioink and cooled at 4 °C. The bioink was then extruded through an 18-G nozzle under different pneumatic pressures to generate a droplet array in a 96-well plate. The printed constructs were cured for 40 s under 405 nm. Subsequently, the organoid medium was added to the 96-well plate and incubated at 37°C (Table 1).

Table 1. 3D bioprinting parameters for DKM–Ru/SPS bioink.

Parameter	Value/range
Bioink temperature in the syringe	4°C
Nozzle gauge (inner diameter)	18 G
Extrusion mode	Pneumatic
Extrusion pressure	3 kPa (tested range: 3–10 kPa)
Printing speed	3–5 mm s^{-1}
Photocrosslinking wavelength	405 nm
Light intensity	30 mW cm^{-2}
Exposure time	40 s
Array format	12 × 8 (96-well plate compatible)

Abbreviations: DKM: Decellularized kidney extracellular matrix; Ru/SPS: Tris(2,2'-bipyridyl) ruthenium (II) chloride hexahydrate/sodium persulfate.

2.8. Statistical analysis

All data are reported as the mean ± standard error of the mean and were derived from at least three biological replicates. Statistical analyses were performed using GraphPad Prism 10.4.3 (San Diego, CA, USA, employing Student's *t*-tests for paired comparisons and one-way or two-way ANOVA for multiple-group assessments. Statistical significance was defined as $^{*}p < 0.05$, $^{**}p < 0.01$, $^{***}p < 0.001$, and $^{****}p < 0.0001$.

3. Results and discussion

3.1. Preparation and characterization of DKM bioink

Decellularized extracellular matrix hydrogels face numerous challenges, including poor mechanical properties, limited printability, and extended gelation duration, which have restricted their application in organoid culture and pharmacological testing. To address these limitations, a tyramine-rich DKM bioink was developed.[30,31] This advanced system integrates a Ru/SPS photoinitiator to enable rapid tyrosine crosslinking, thereby providing an efficient and rapid solution for research. Separately, mouse liver and lung were expanded into organoids and subsequently combined with the DKM–Ru/SPS bioink formulation. Using 3D bioprinting, the organoid-embedded bioink was precisely deposited into 96-well plates (Figure 1).

In addition, the high biocompatibility of the DKM bioink, coupled with its rapid light-triggered crosslinking capability (~40 s with Ru/SPS), was demonstrated to effectively minimize cell stress during printing while maintaining organoid viability. This innovative light-triggered crosslinking strategy, combined with 3D bioprinting, is thus established as a promising platform for fabricating complex hydrogel-based tissues and advancing organoid culture systems for diverse therapeutic and diagnostic applications.

Decellularized tissues have been regarded as promising biomaterials for replicating the complex native ECM microenvironment, given their similarity to native tissues. This similarity is primarily attributed to the preservation of organ-specific biochemical composition (e.g., collagens, laminin), native 3D architecture, and critical mechanical properties.[32] Kidney tissue was harvested and analyzed for its microstructural features and compositional characteristics. To achieve this, the tissue was sectioned into small fragments, subjected to detergent-based decellularization, and subsequently lyophilized. Upon temperature equilibration under physiological conditions (37°C), decellularized DKM solutions exhibited temperature-dependent solution–gel transitions, ultimately yielding robust and well-defined hydrogels (Figure 2A).

Decellularization efficacy was verified through SEM, H&E, and immunofluorescence staining. SEM confirmed that the kidney tissue exhibited a fibrous, mesh-like morphology following decellularization, indicative of successful cellular removal while preserving structural integrity (Figure 2B). H&E staining for cellular components and 4',6-diamidino-2-phenylindole fluorescence staining for nuclear material detection were performed. Prior to decellularization, stained sections showed collagen (blue) alongside extensive red staining, indicating the presence of muscle fibers. After decellularization, tissue sections primarily exhibited blue coloration with no visible red fibers, demonstrating effective removal of cellular muscle components while retaining the collagen matrix, thereby confirming the efficacy of the decellularization process (Figure 2C). Moreover, immunohistochemical analysis confirmed the preservation and structural integrity of key ECM components, including collagen I, collagen IV, laminin, and fibronectin after decellularization (Figure 2D).

Quantitative analysis of DNA content was conducted to evaluate the efficiency of cellular component removal, demonstrating a statistically significant reduction in decellularized tissue relative to native tissue ($p < 0.001$), corresponding to a 95.1% decrease in residual DNA content. To assess ECM preservation, quantitative analyses demonstrated that collagen content in decellularized tissue increased to 1,431 μg mg^{-1} compared with 314 μg mg^{-1} in native tissue, representing an approximately 4.6-fold increase in relative abundance, attributable to the efficient removal of cellular materials. Meanwhile, GAG content was retained at 65.55% relative to native tissue. Collectively, these results show that the protocol effectively removed cellular remnants while preserving critical ECM components (Figure 2E).

The presence of growth factors in the DKM solution was confirmed following the decellularization process. After treatment, the concentrations were measured as follows: IGF-1, 130.00 ± 17.21 ng/mL; EGF, 0.8007 ± 0.0299 ng/mL; and TGF-β, 1.6693 ± 0.04833 ng/mL. These values were comparable to those measured before decellularization: IGF-1, 130.08 ± 5.57 ng/mL; EGF, 0.7851 ± 0.0648 ng/mL; and TGF-β, 1.4550 ± 0.3073 ng/mL (Figure S1A). Previous studies have indicated that IGF-1 and EGF promote development and inhibit apoptosis, while TGF-β has been implicated in regulating cell formation and inhibiting differentiation.[33-34] These results indicate that growth factors were effectively retained throughout the decellularization process. The elevated concentrations of IGF-1, EGF, and TGF-β in DKM may provide an optimal environment and underlie the successful culture of organoids.

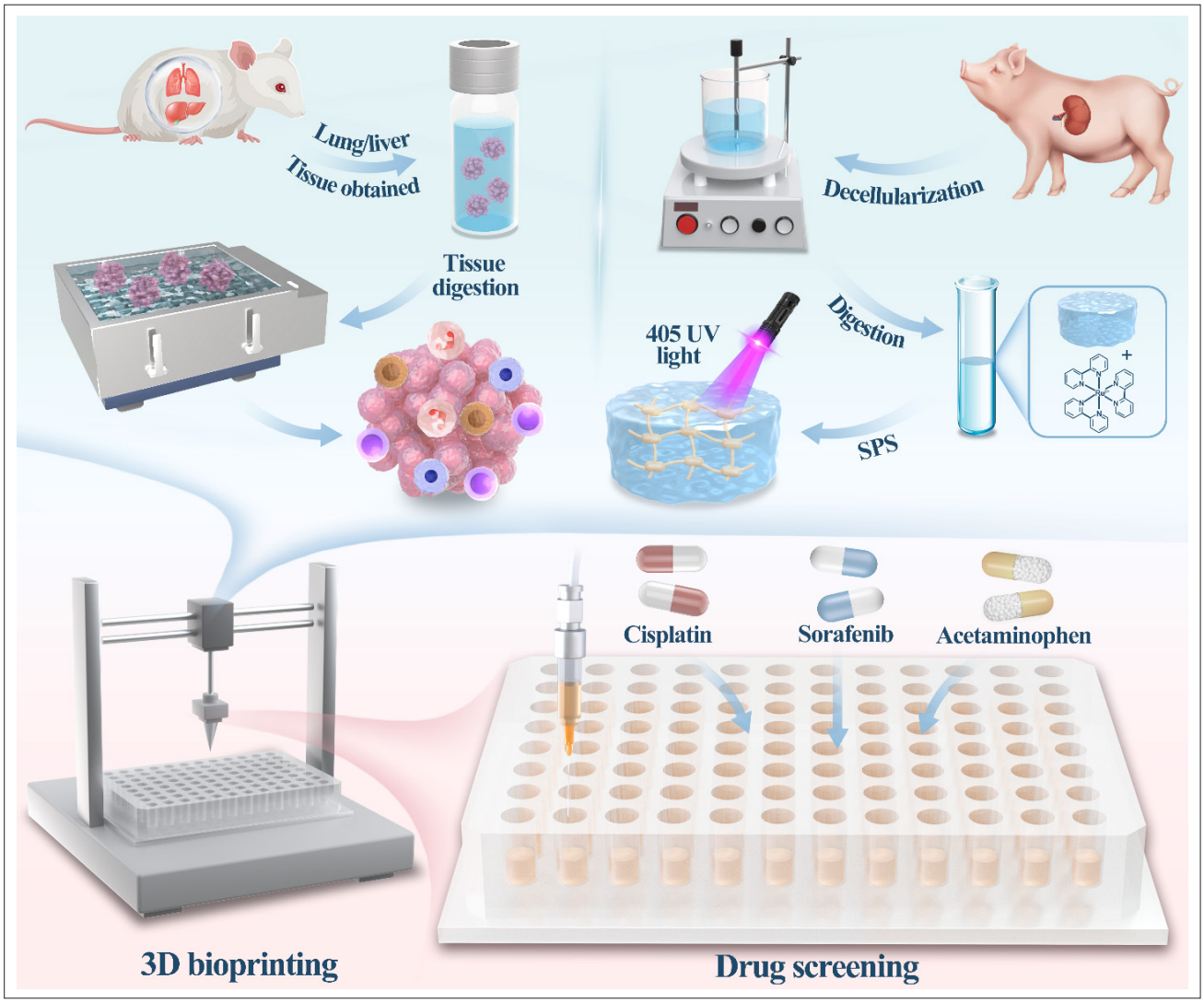

Figure 1. Schematic illustrating the DKM–Ru/SPS bioink preparation and 3D bioprinting procedures. Porcine kidney tissue was decellularized to produce the DKM solution. The DKM solution was mixed with Ru/SPS to initiate the photocrosslinking process. Mouse-derived cells (digested and isolated) were embedded within the DKM–Ru/SPS bioink, followed by photocrosslinking. Using a 3D bioprinter, the cell-laden bioink was deposited into a 96-well plate to form bioprinted organoids, which were subsequently subjected to drug screening. Abbreviations: DKM: Decellularized kidney extracellular matrix; Ru: Tris(2,2'-bipyridyl) ruthenium (II) chloride hexahydrate; SPS; Sodium persulfate UV: Ultraviolet.

To assess the biocompatibility of the DKM, potential residual contaminants were also quantified. Endotoxin levels were measured at 0.08,245 ± 0.01,288 EU/mL for lot 1, 0.03,601 ± 0.00,255 EU/mL for lot 2, and 0.04,708 ± 0.02,985 EU/mL for lot 3. Endotoxin analysis across three DKM lots revealed levels below the FDA limit of 0.5 EU/mL (Figure S1B).[35] Furthermore, residual SDS concentrations were measured as 0.000,597 ± 0.000,524 mg/mL for lot 1, 0.002,598 ± 0.001,637 mg/mL for lot 2, and 0.001,565 ± 0.001,003 mg/mL for lot 3. The residual SDS content was determined to be below 0.005 mg/mL (Figure S1C). Collectively, these results demonstrate that our protocol yielded a safe, biocompatible, and ECM-rich material suitable for bioink formulation.

3.2. Rheological characterization of DKM–Ru/SPS bioink

Numerous prior studies have indicated that a Ru-to-SPS ratio of 1:10 is optimal for efficient crosslinking. Guided by this, we designed a series of concentration proportions. The physical characterization of light-crosslinked bioink was assessed as a function of both DKM bioink concentration (10, 15, 20 mg/mL) and Ru/SPS photoinitiator concentration (0.125, 0.25, 0.5 mM). The morphological integrity of the DKM–Ru/SPS bioinks was evaluated over

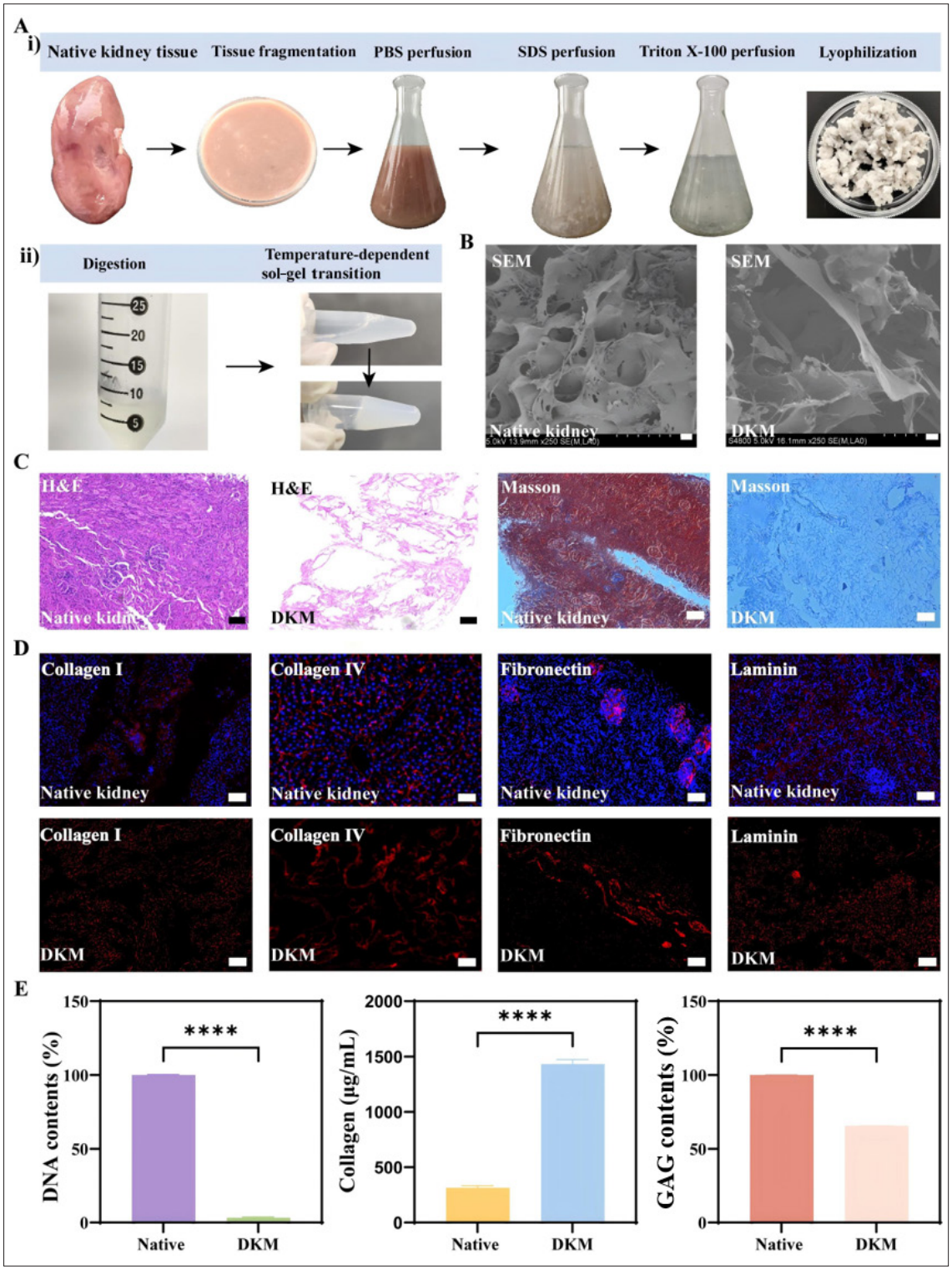

Figure 2. Structural and compositional analysis of the kidney scaffold before and after decellularization. (A) Schematic illustration of DKM (i) bioink fabrication and (ii) gel transition process. (B) Scanning electron microscopy (SEM), (C) hematoxylin and eosin (H&E) and Masson's trichrome staining, and (D) immunofluorescence staining of extracellular matrix components (laminin, fibronectin, and collagen) before and after decellularization. All sections were counterstained with 4',6-diamidino-2-phenylindole (blue). Scale bar: 200 μm; magnification: 4×. (E) Quantitative analysis of DNA, collagen, and glycosaminoglycan (GAG) content before and after the decellularization process. Notes: $n = 3$; mean ± standard error of the mean; ****$p < 0.0001$. Abbreviations: DKM, Decellularized kidney extracellular matrix; PBS, Phosphate-buffered saline; SDS, Sodium dodecyl sulfate.

a 20-day period in well plates. Representative images (Figure 3Ai) show that all bioink formulations maintained their original, well-defined circular morphology without noticeable disintegration. Quantitative analysis of diameter (Figure 3Aii) and area (Figure 3Aiii) confirmed these observations, revealing no statistically significant changes in bioink dimensions during culture. This long-term stability under physiological conditions is a critical attribute for bioinks, as it ensures that the printed constructs can serve as durable and reliable scaffolds throughout the crucial phases of cell proliferation and tissue maturation. The preserved integrity of the bioinks provided a consistent 3D architecture for potential cellular ingrowth and organization.

We then characterized the bioink's rheological properties. As illustrated in Figure 3B, visual inspection revealed a progressive reduction in droplet size with increasing concentrations of either DKM or Ru/SPS, indicating the formation of a denser and more compact crosslinked network. This observation was further substantiated by mechanical analysis (Figure 3C), which confirmed the formation of a solid-like hydrogel, as the storage modulus (*G*') consistently exceeded the loss modulus (*G*") across all tested frequencies. Importantly, the stiffness was tunable and increased significantly with higher DKM concentrations (e.g., 20 > 15 > 10 mg/mL).

A higher concentration of DKM provides more available crosslinking sites, while a higher concentration of the Ru/SPS system generates a greater number of free radicals upon illumination. Visible-light Ru/SPS systems have been widely applied for the rapid photocrosslinking of gelatin-based and dECM-derived hydrogels with improved print fidelity and cell compatibility.[36–37] Our DKM–Ru/SPS formulation extends these approaches to a kidney-specific dECM, providing a fast and mild crosslinking strategy while preserving native ECM composition. These factors act synergistically to promote rapid and extensive radical polymerization, resulting

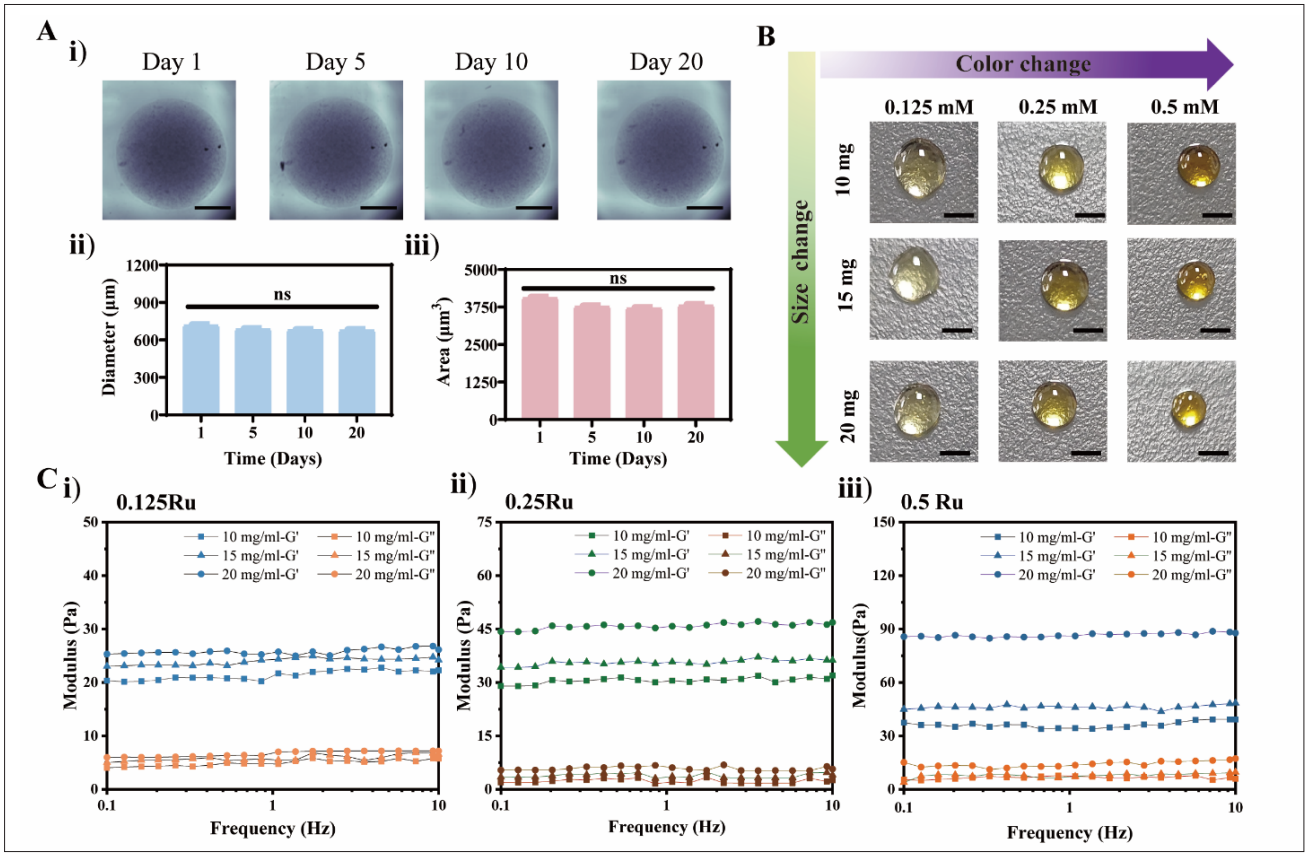

Figure 3. Microstructural, physical, and chemical analysis of DKM–Ru/SPS bioinks. (A) (i) Morphological characterization of bioinks immersed in a 24-well plate for 20 days and analysis of (ii) diameter and (iii) area of bioinks. Scale bar = 2 mm. Data are representative of three independent experiments (n = 3). (B) Photographic images of DKM– Ru/SPS bioink (10, 15, 20 mg/mL) with varying Ru/SPS concentrations (0.125, 0.25, 0.5 mM). Scale bar = 5 mm. (C) Rheological assessment of DKM–Ru/SPS bioinks at different concentrations: (i–iii) shear-thinning characteristics. Abbreviations: DKM; Decellularized kidney extracellular matrix; *G*', Storage modulus; *G*", Loss modulus; ns: Not statistically significant; Ru/SPS; Tris(2,2'-bipyridyl) ruthenium (II) chloride hexahydrate/sodium persulfate.

in a tighter polymer network that undergoes greater contraction upon gelation. This tunability enables precise control over scaffold properties through simple adjustment of the initial composition, thereby allowing the customization of the bioink to support specific tissue microenvironments.

A bioink must possess appropriate physical properties to ensure successful bioprinting and long-term culture. We therefore examined the gelation kinetics of the DKM–Ru/SPS bioink (Figure S2). While pure DKM and Matrigel exhibited slow, temperature-dependent gelation (~30 min at 37°C), the DKM–Ru/SPS bioink, in addition to this thermoresponsive behavior, could be rapidly light-crosslinked into a stable hydrogel within ~40 s using 405 nm light. This rapid light-crosslinking capability is critical for stabilizing printed structures while maintaining cell viability. The DKM–Ru/SPS bioink exhibited significantly enhanced mechanical properties through optimized visible light-mediated crosslinking. As illustrated in Figure S3, direct crosslinking resulted in a Young's modulus of 22.76 ± 1.91 kPa, representing an approximately fourfold increase compared with thermal gelation alone. Notably, this stiffness exceeds the typical modulus range of widely used commercial hydrogels, such as Matrigel, thereby providing a mechanically superior alternative for 3D bioprinting applications.

3.3. Printability and biocompatibility optimization of DKM–Ru/SPS bioink

To identify the optimal formulation, mechanical performance was balanced against cytocompatibility. As illustrated in Figure S4, cell viability exceeded 98%, demonstrating the good biocompatibility of the DKM bioink. L929 cells were cultured in bioinks with graded crosslinker concentrations. At a fixed Ru/SPS ratio of 0.125:1.25 mM, cell viabilities in bioinks containing 10, 15, and 20 mg/mL DKM were 98.04 ± 2.23%, 98.61 ± 1.01%, and 98.62 ± 0.84% on Day 7, respectively. When the Ru/SPS ratio was increased to 0.25:2.5 mM, viabilities improved to 99.21 ± 0.68%, 99.316 ± 0.212%, and 99.363 ± 0.283%. In contrast, at a Ru/SPS ratio of 0.5:5 mM, cell viability decreased substantially to 64.79 ± 1.03%, 82.37 ± 2.17%, and 95.22 ± 2.15% across the same DKM concentrations. While Ru/SPS ratios of 0.125 and 0.25 mM supported excellent cellular survival (>98%), the 0.5 mM ratio induced significant dose-dependent cytotoxicity (Figure 4A–C).

Further evaluation of cell encapsulation within the composite DKM–Ru/SPS bioink revealed that increasing Ru/SPS concentration correlated with reduced cell viability. Conversely, higher DKM concentrations partially mitigated this cytotoxic effect, likely due to their cytoprotective properties and increased availability of crosslinking sites, which may shield cells from excessive free radical exposure. A Ru/SPS ratio above a 0.25:2.5 mM was therefore detrimental to cell survival, irrespective of DKM concentration.

Following cytocompatibility assessment, printing parameters for cell-laden bioinks were optimized. The rheological behavior of the DKM–Ru/SPS bioink, which is essential for 3D bioprinting, was highly dependent on composition. In particular, the 0.25 Ru/SPS formulation demonstrated pronounced shear-thinning behavior, facilitating smooth extrusion, as well as temperature-dependent gelation. Furthermore, viscosity increased proportionally with DKM concentration (10, 15, and 20 mg/mL) (Figure 4D), a trend attributed to the dense macromolecular network of the dECM. This inherent viscosity and tunable viscosity, even at relatively low concentrations, are advantageous for achieving high structural fidelity in printed constructs.[38] Collectively, these rheological characteristics enhance the broader applicability of the DKM-based biomaterial for biomedical use. Based on these findings, the 0.25 mM Ru/2.5 mM SPS ratio was selected as the optimal formulation, providing rapid gelation and robust mechanics without compromising cell viability.

Printability analysis under varying extrusion pressures (3, 5, and 10 kPa) demonstrated precise control over droplet dimensions: at a fixed bioink concentration, droplet size increased with higher pressure, while at constant pressure, droplet size decreased with increasing bioink concentration (Figure 4E). Through optimization of extrusion pressure (3 kPa) and DKM concentration, multiple replicas with precise dimensions were fabricated. The DKM bioink maintained sufficient viscosity during *in situ* printing, ensuring accurate deposition and structural fidelity. Consequently, the 0.25 mM Ru/SPS DKM bioink, with its favorable biofunctional characteristics and adaptable rheological properties, represents a promising material for advanced 3D bioprinting applications. In comparison, manually dispensed droplets exhibited irregular shapes and significant size variability, whereas 3D-printed droplets were uniform in both morphology and diameter (Figure S5). This result demonstrates that 3D bioprinting offers significantly enhanced stability and control over droplet size compared with manual dispensing. Such reproducibility is critical for ensuring consistent cell encapsulation and deposition, thereby supporting high cell viability and the formation of predictable, functional tissue constructs.

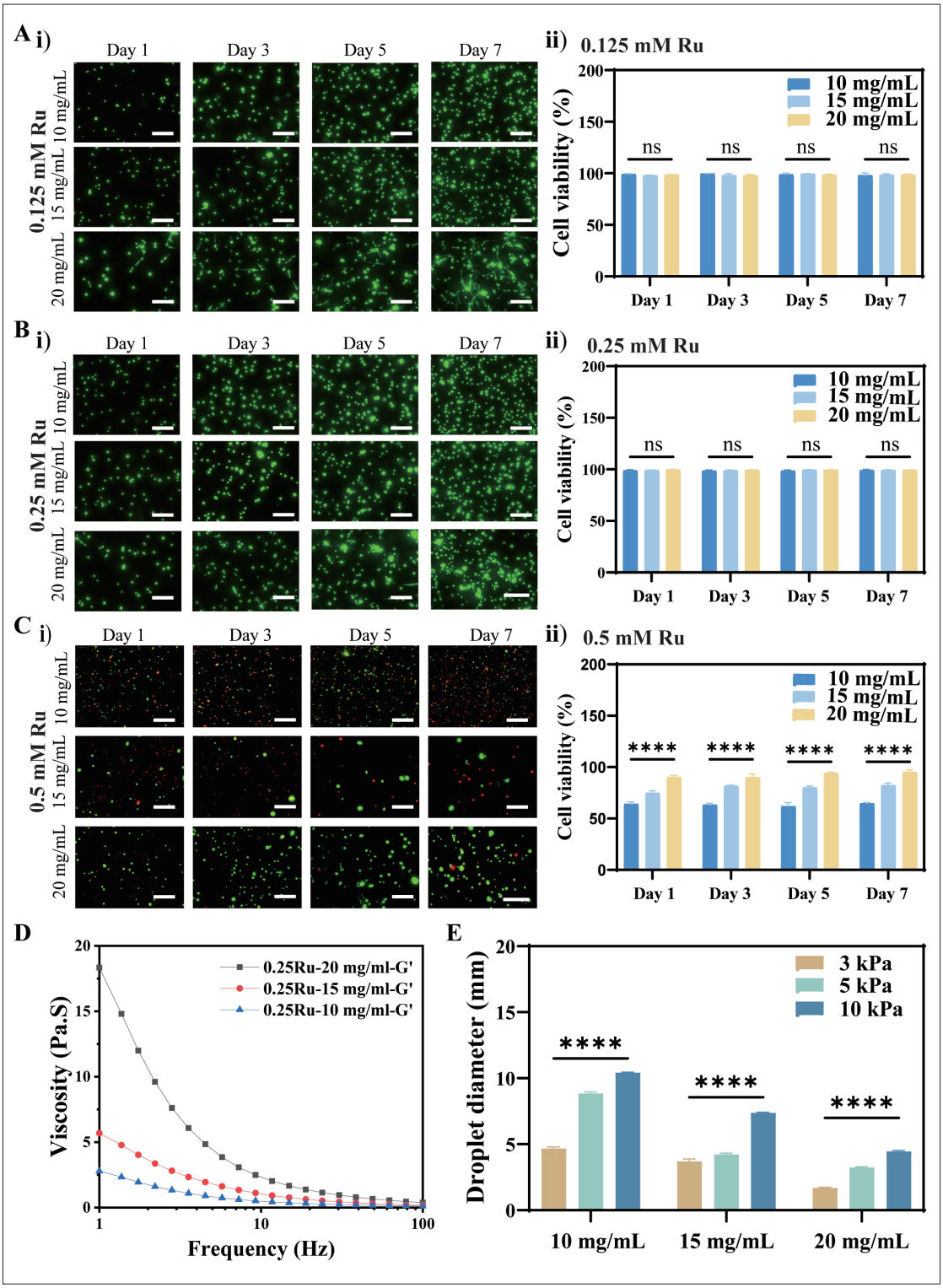

Figure 4. Biocompatibility and printability assessment of DKM–Ru/SPS bioink with varying crosslinker concentrations. (A–C) (i) Representative fluorescence images and (ii) quantitative assessment of live/dead cell viability in L929 cells over 7 days with Ru/SPS concentrations of 0.125, 0.25, and 0.5 mM. Scale bar: 300 μm; magnification: 4×. (D) Viscosity profiles of bioinks at different concentrations under shear strain. (E) Analysis of droplet dimensions at extrusion pressures of (i) 3 kPa, (ii) 5 kPa, and (iii) 10 kPa across different bioink concentrations. Notes: Data are presented as mean ± standard error of the mean; ****$p < 0.0001$; $n = 3$. Abbreviations: DKM, Decellularized kidney extracellular matrix; *G'*, Storage modulus; ns, Not statistically significant; Ru/SPS, Tris(2,2'-bipyridyl) ruthenium (II) chloride hexahydrate/sodium persulfate.

3.4. Assessment of DKM–Ru/SPS bioink for 3D lung organoid culture and bioprinting

To evaluate the performance of our developed DKM–Ru/SPS bioink for 3D culture, we systematically applied it to lung organoid cultivation and compared its efficacy with that of Matrigel. We first investigated the effect of DKM–Ru/SPS bioink concentration on organoid formation. Mouse lung organoids were embedded in bioinks with varying concentrations (10, 15, and 20 mg/mL). Although organoids formed under all tested conditions, quantitative analysis revealed that the 15 mg/mL formulation yielded the highest formation efficiency and optimal organoid diameter, establishing it as the optimal concentration for subsequent experiments (Figure 5Ai–ii). We next compared organoid growth in the DKM–Ru/SPS bioink with that in Matrigel. Organoids cultured in the base DKM–Ru/SPS bioink grew effectively but exhibited lower formation efficiency than those cultured in Matrigel. Notably, supplementation of the DKM–Ru/SPS bioink with 0.1 mg/mL laminin resulted in a significant improvement. The diameter of organoids grown in DKM–Ru/SPS–laminin were comparable to those cultured in Matrigel, and their formation efficiency showed no statistically significant difference relative to the Matrigel control, indicating that laminin is a crucial component for maximizing bioink performance (Figure 5Bi–ii). The superior organoid formation observed at 15 mg/mL indicates that this concentration provides optimal biophysical support for lung organoid development. Furthermore, marked enhancement achieved through laminin supplementation confirms that specific ECM components are essential for maximizing bioink functionality. Collectively, the comparable performance between the optimized DKM–Ru/SPS–laminin formulation and Matrigel validates its effectiveness for lung organoid culture. Beyond supporting organoid growth, Matrigel has been widely used to mimic the tumor microenvironment for *in vitro* disease modeling.[39–40] Considering the demonstrated ability of our DKM–Ru/SPS bioink to support both liver and lung organoid culture, this dECM-based visible-light-crosslinkable bioink may serve as a versatile platform for mimicking disease-associated microenvironments and for investigating how ECM conditions regulate organoid behavior.

The viability of organoids cultured in the DKM–Ru/SPS bioink was further assessed using live/dead staining (Figure S6). Although viability in the DKM–Ru/SPS was slightly lower than that in Matrigel on Day 1, by Day 5, the bioink supported organoids with viability exceeding 95%, with no statistically significantly different compared to Matrigel, demonstrating excellent biocompatibility (Figure 5C). To assess long-term culture capacity, lung organoids embedded in the DKM–Ru/SPS bioink were serially passaged. Representative bright-field images confirmed successful formation and robust growth of organoids over multiple passages, up to passage 8, indicating that the bioink supports stable and sustained development without compromising growth potential (Figure 5D). To further demonstrate the versatility and practical applicability of the DKM–Ru/SPS bioink, we employed 3D bioprinting to fabricate lung organoid constructs with defined architectures. As shown in Figure S7A, lung organoid-laden bioink was successfully printed into a predefined array within a 96-well plate. After 10 days of culture, bright-field imaging revealed that the printed organoids maintained structural integrity and exhibited robust growth and development, confirming the excellent printability and printing compatibility of the bioink.

Subsequent histological and immunohistochemical analyses were performed to further characterize organoids cultured within the printed bioink constructs. H&E staining revealed the formation of complex cyst-like structures containing multiple lumens, a hallmark of well-developed organoids. Immunohistochemical analysis further confirmed positive expression of key lung lineage markers, including TTF-1 and P63. The presence of these distinct cell populations (Figure S7B) conclusively demonstrates effective differentiation and maturation of lung organoids within the 3D-printed DKM–Ru/SPS bioink, underscoring its utility as a biomimetic platform for engineering physiologically relevant tissue models.

3.5. Evaluation of DKM–Ru/SPS bioink for liver organoid culture and drug screening

After demonstrating its efficacy in lung organoid cultures, we next assessed the broader applicability of the DKM–Ru/SPS bioink for the culture and pharmacological testing of mouse primary liver organoids. Figure 6A presents a schematic overview of the integrated workflow, illustrating the progression from organoid fabrication using a 3D bioprinter to high-throughput drug screening. Liver organoids cultured in the DKM–Ru/SPS bioink exhibited substantial growth and characteristic morphological development from Days 1 to 7, comparable to organoids cultured in Matrigel (Figure 6B). Quantitative analysis demonstrated that both organoid diameter and formation efficiency in the DKM–Ru/SPS bioink were not significantly different from those observed in Matrigel throughout the culture period (Figure 6C), highlighting the bioink's strong support for liver organoid proliferation and development. Additionally, viability assessment via live/dead staining after 7 days of culture further revealed that liver organoids maintained high cell viability (>95%) within the DKM–Ru/SPS bioink (Figure S8), comparable to Matrigel controls.

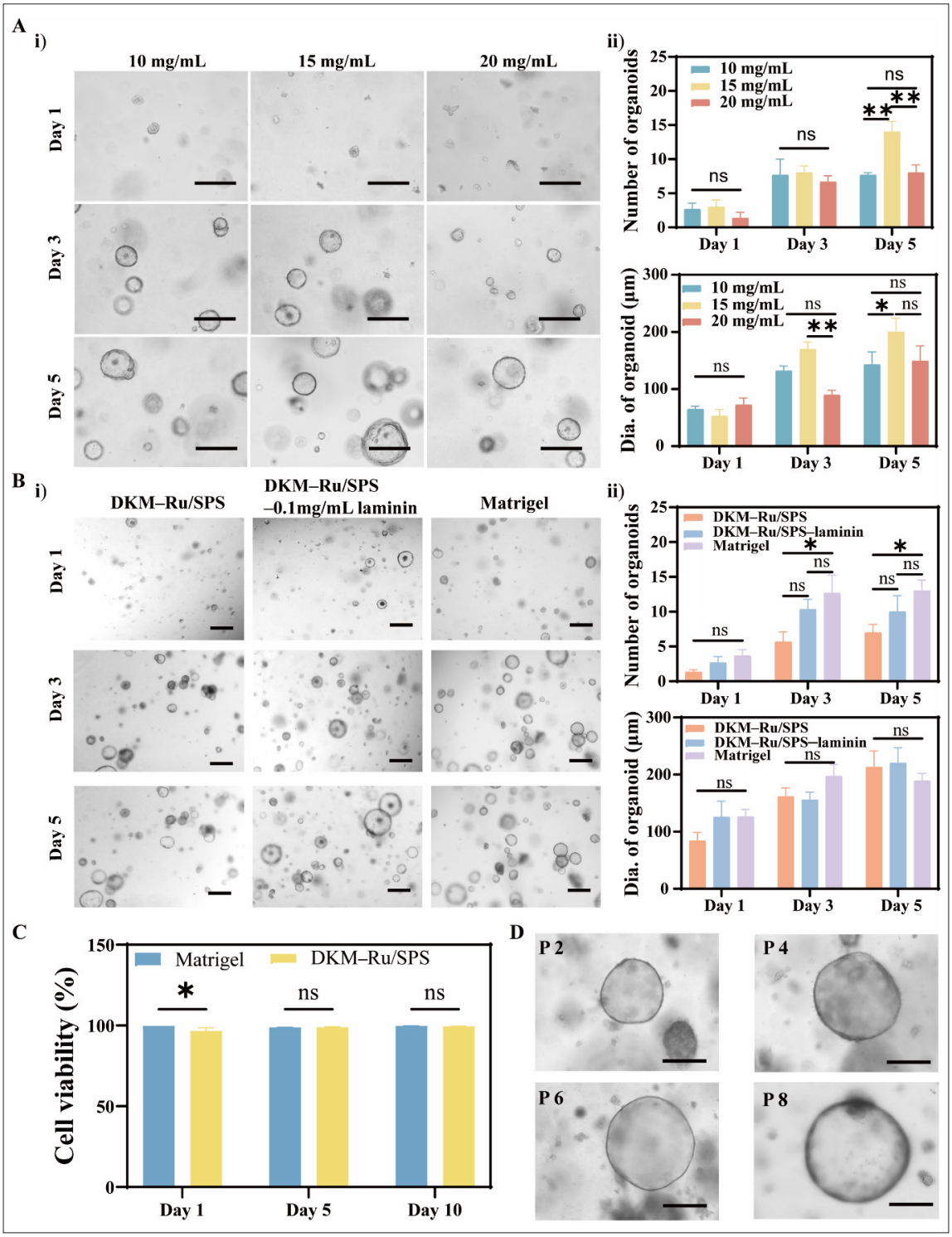

Figure 5. Characterization of lung organoid growth, viability, and development in DKM–Ru/SPS bioink. (A) (i) Bright-field images of lung organoids cultured in various concentrations of DKM–Ru/SPS bioink at Day 5 and (ii) quantitative analysis of organoid size and formation efficiency. Scale bar = 300 μm; magnification: 4×. (B) (i) Organoids seeded in DKM–Ru/SPS, DKMRu/SPS –laminin, and Matrigel for 5 days with (ii) corresponding quantitative measurements. Scale bar = 300 μm; magnification: 4×. (C) Live/dead viability analysis of organoids cultured in DKM–Ru/SPS bioinks and Matrigel. (D) Representative bright-field images of lung organoids formation at passage 2, 4, 6, and 8. Scale bar: 300 μm; magnification: 40×. Notes: $n = 3$; mean ± standard error of the mean; one-way analysis of variance; $^{*}p < 0.05$, $^{**}p < 0.01$. Abbreviations: Dia, Diameter; DKM: Decellularized kidney extracellular matrix; ns: Not statistically significant; Ru/SPS; Tris(2,2'-bipyridyl) ruthenium (II) chloride hexahydrate/sodium persulfate.

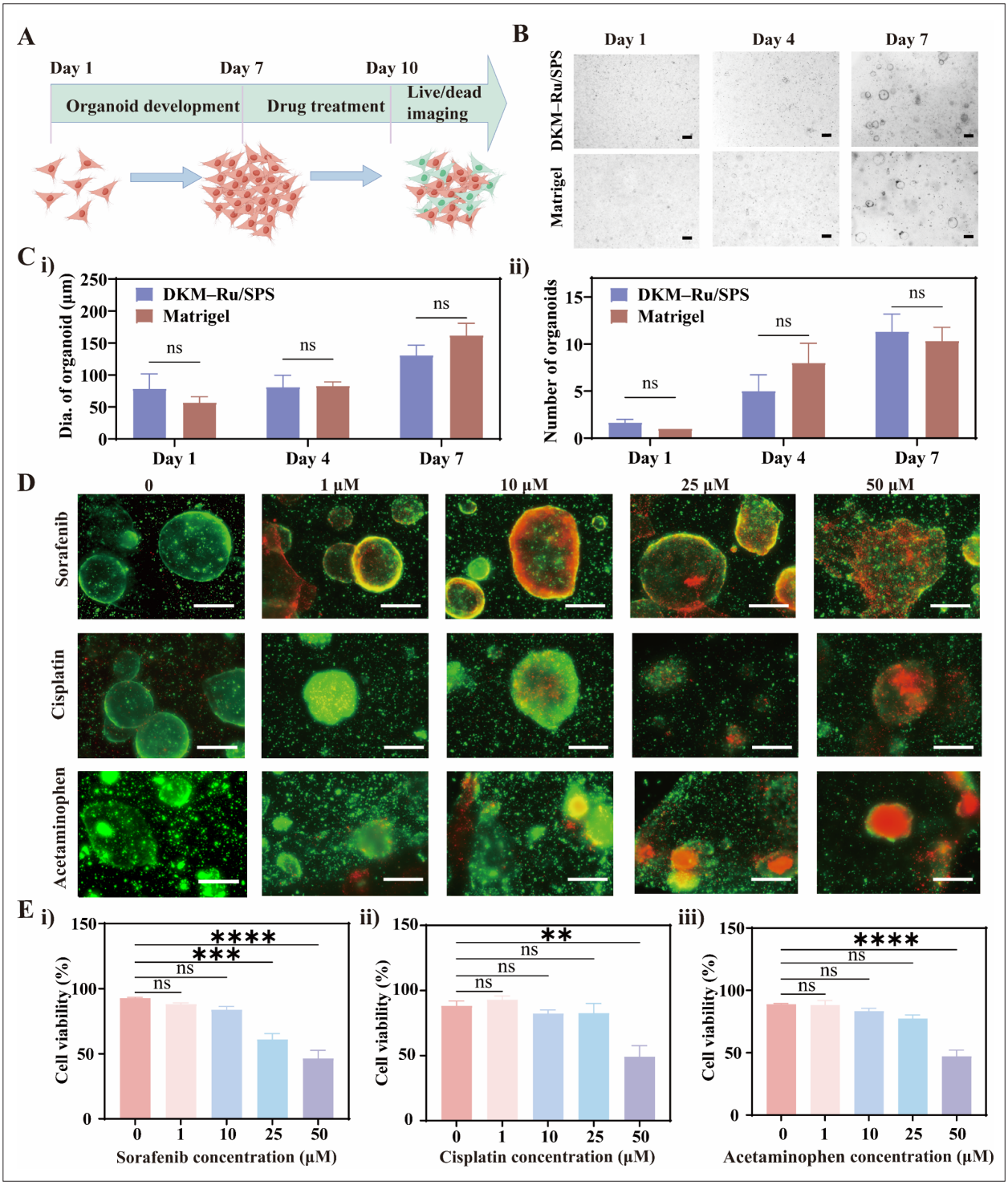

Figure 6. Application of DKM–Ru/SPS bioink for liver organoid culture and drug screening. (A) Schematic illustration of organoid fabrication and drug screening using a 3D bioprinter. (B) Culture of mouse primary liver organoids (P0) in DKM–Ru/SPS bioink and Matrigel, with representative bright-field images captured at 4× magnification from Days 1 to 7. Scale bar = 300 μm. (C) Quantification of (i) organoid size and (ii) formation efficiency from panel B. (D) Live/dead staining of liver organoids treated with increasing doses (1–50 μM) of sorafenib, cisplatin, and acetaminophen. Scale bar = 300 μm; magnification: 40×. (E) Quantitative analysis of live/dead staining for (i) sorafenib, (ii) cisplatin, and (iii) acetaminophen. Notes: Data are representative of three independent experiments (n = 3); mean ± standard error of the mean, one-way analysis of variance; ****p < 0.0001, ***p < 0.001, **p < 0.01. Abbreviations: Dia, Diameter; DKM: Decellularized kidney extracellular matrix; ns: Not statistically significant; Ru/SPS; Tris(2,2'-bipyridyl) ruthenium (II) chloride hexahydrate/sodium persulfate.

This robust growth was also confirmed in the context of 3D bioprinting, as representative bright-field images obtained after 7 days showed well-developed and healthy liver organoids embedded within printed DKM–Ru/SPS bioink structures arranged in a 96-well plate (Figure S9). These observations confirm both the structural integrity of the printed constructs and the functional viability of the organoids.

As a proof of concept for drug screening, sorafenib, cisplatin, and acetaminophen were selected as representative hepatotoxic compounds. Quantitative analysis of live/dead staining (Figure 6D and E) revealed a dose-dependent decrease in cell viability for all three compounds. Following treatment, liver organoid viability after exposure to sorafenib at 0, 1, 10, 25, and 50 μM was 92.73 ± 1.09%, 88.12 ± 1.73%, 83.84 ± 4.31%, 61.06 ± 7.62%, and 46.23 ± 11.10%, respectively. For cisplatin at the same concentrations, viability was 88.27 ± 6.42%, 92.84 ± 5.20%, 82.24 ± 4.89%, 82.61 ± 13.02%, and 49.08 ± 14.72%. Similarly, acetaminophen treatment resulted in viabilities of 90.26 ± 0.3%, 88.23 ± 6.36%, 83.42 ± 3.90%, 77.43 ± 5.03%, and 47.04 ± 8.71%. In all experiments, viability in untreated control groups (0 μM) remained above 90%. Statistically significant toxicity ($p < 0.05$) was observed at 25 and 50 μM for sorafenib and at 50 μM for both cisplatin and acetaminophen, confirming the platform's sensitivity for drug toxicity screening.

The effective implementation of drug testing in this study serves two critical objectives. It confirms that the DKM–Ru/SPS bioink creates a universally applicable and physiologically responsive microenvironment that not only promotes the growth of various organoid types, including lung and liver organoids, but also facilitates their maturation for pharmacological investigations. Furthermore, liver organoids exhibited significant dose-dependent responses to both hepatocyte-specific drugs (acetaminophen) and broad-spectrum chemotherapeutic agents (cisplatin), indicating that this platform has strong potential for diverse toxicity screening applications.

The present work establishes DKM–Ru/SPS as a visible-light-crosslinkable bioink with broad potential applications. In future studies, this dECM-based bioink could be combined with patient-derived organoids to enable personalized drug sensitivity testing within a tissue-mimetic ECM. Integration with microfluidic organ-on-a-chip platforms may further enable incorporation of perfusion, mechanical cues, and multiorgan interactions, as advocated for next-generation functional hydrogels and microphysiological systems.[37] Additionally, systematic tuning of DKM content and Ru/SPS concentration could facilitate modeling of progressive fibrosis or desmoplastic tumor stroma, enabling investigation of how such matrices, in combination with tumor microenvironment-responsive nanomedicines, regulate immune responses and therapeutic resistance.[39,40]

4. Conclusion

In conclusion, this study establishes a visible-light-crosslinkable DKM bioink integrated with the Ru/SPS photoinitiator system as a robust and versatile platform for 3D bioprinting and organoid culture. The key innovation lies in its ability to achieve rapid photocrosslinking within 40 s, representing a significant advancement over conventional thermosensitive dECM hydrogels. This system enables high-fidelity bioprinting of organoid-laden constructs and effectively supports the growth and maturation of lung and liver organoids, with performance comparable to that of Matrigel. Furthermore, its successful application in hepatoxicity assessment demonstrates its potential for drug testing using an *in vitro* biomimetic platform. By addressing critical limitations related to gelation kinetics and printability, the DKM–Ru/SPS bioink not only broadens the biomedical applications of dECM-derived biomaterials but also paves the way for standardized, automated, and high-throughput organoid-based models for drug discovery and regenerative medicine.

Acknowledgments

None.

Funding

The authors acknowledge the financial support from the National Key Research and Development Program of China (Nos. 2022YFA1105200 and 2022YFB3804700), the Central Government Guiding Local Science and Technology Development Special Fund Projects in Sichuan Province (No. 2023ZYD0166), the Chengdu City Science and Technology Project of "Unveiling and Commanding" (No. 2024-JB00-00018-GX), and the Eastern New District of Chengdu for the Implementation of Technological Innovation Projects (No. 2024-DBXQ-KJYF002).

Conflict of interest

The authors declare no conflicts of interest.

Author contributions

Conceptualization: Wenqi Hu, Chengwei Sun, Haijie Hu, Litian Zhao, Zipeng Yao, Shuqi Wang
Formal analysis: Guohua Wu, Mengjiao Xia, Di Wu
Investigation: Wenqi Hu, Guohua Wu, Mengjiao Xia, Di Wu
Methodology: Wenqi Hu

Writing–original draft: Qijun Du, Qinrui Lu, Jiashu Wang
Writing–review & editing: Ao Xie, Chengwei Sun, Haijie Hu, Litian Zhao, Zipeng Yao, Shuqi Wang

Ethics approval and consent to participate

All animal experiments were approved by the West China Hospital Animal Care Ethics Committee (Approval No. 108, 2023).

Consent for publication

Not applicable.

Availability of data

The raw data supporting the findings of this study are available from the corresponding author upon reasonable request.

References

1. Frankell AM, Dietzen M, Al Bakir M, *et al*. The evolution of lung cancer and impact of subclonal selection in TRACERx. *Nature*. 2023;616(7957):525-533. doi: 10.1038/s41586-023-05783-5
2. Lian L, Xie M, Luo Z, *et al*. Rapid volumetric bioprinting of decellularized extracellular matrix bioinks. *Adv Mater*. 2024;36(34):2304846. doi: 10.1002/adma.202304846
3. Kratochvil MJ, Seymour AJ, Li TL, Paşca SP, Kuo CJ, Heilshorn SC. Engineered materials for organoid systems. *Nat Rev Mater*. 2019;4(9):606-622. doi: 10.1038/s41578-019-0129-9
4. Xie M, Sun Y, Wang J, *et al*. Thermo-sensitive sacrificial microsphere-based bioink for centimeter-scale tissue with angiogenesis. *IJB*. 2022;8(4):599. doi: 10.18063/ijb.v8i4.599
5. Liu J, Wu G, Wu D, *et al*. Microfluidic organoid-slice-on-a-chip system for studying anti-cholangiocarcinoma drug efficacy and hepatorenal toxicity. *Lab Chip*. 2025;25(12): 2839-2850. doi: 10.1039/D4LC00902A
6. Wu G, Wu D, Hu W, *et al*. A novel microfluidic self-perfusion chip (MSPC) for pumpless 3D cell, microtissue and organoid culture. *Lab Chip*. 2025;25(15):3694-3706. doi: 10.1039/D5LC00030K
7. Hu W, Bei HP, Jiang H, *et al*. DLM–GelMA/tumor slice sandwich structured tumor on a chip for drug efficacy testing. *Lab Chip*. 2024;24(15):3718-3727. doi: 10.1039/D4LC00278D
8. Wu M, Huang K, Long C, Yang C, Tong Y. In vitro extracellular matrix model to evaluate stroma cell response to transvaginal mesh. *Neurourol Urodyn*. 2013;33(4):449-454. doi: 10.1002/nau.22425
9. Song H, Jiang H, Hu W, *et al*. Cervical extracellular matrix hydrogel optimizes tumor heterogeneity of cervical squamous cell carcinoma organoids. *Sci Adv*. 2024;10(20):eadl3511. doi: 10.1126/sciadv.adl3511
10. Kim J, Kim J, Gao G, *et al*. Bioprinted organoids platform with tumor vasculature for implementing precision personalized medicine targeted towards gastric cancer. *Adv Funct Mater*. 2023;34(11):2306676. doi: 10.1002/adfm.202306676
11. Treacy NJ, Clerkin S, Davis JL, *et al*. Growth and differentiation of human induced pluripotent stem cell (hiPSC)-derived kidney organoids using fully synthetic peptide hydrogels. *Bioact Mater*. 2023;21:142-156. doi: 10.1016/j.bioactmat.2022.08.003
12. Lin L, Jiang S, Yang J, *et al*. Application of 3D-bioprinted nanocellulose and cellulose derivative-based bio-inks in bone and cartilage tissue engineering. *IJB*. 2022;9(1):637. doi: 10.18063/ijb.v9i1.637
13. Garreta E, Moya-Rull D, Marco A, *et al*. Natural hydrogels support kidney organoid generation and promote in vitro angiogenesis. *Adv Mater*. 2024;36(34):2400306. doi: 10.1002/adma.202400306
14. Jin Y, Zhang J, Xu Y, *et al*. Stem cell-derived hepatocyte therapy using versatile biomimetic nanozyme incorporated nanofiber-reinforced decellularized extracellular matrix hydrogels for the treatment of acute liver failure. *Bioact Mater*. 2023;28:112-131. doi: 10.1016/j.bioactmat.2023.05.001
15. Wei Q, Liu D, Chu G, *et al*. TGF-β1-supplemented decellularized annulus fibrosus matrix hydrogels promote annulus fibrosus repair. *Bioact Mater*. 2023;19:581-593. doi: j.bioactmat.2022.04.025
16. Zhang X, Chen X, Hong H, Hu R, Liu J, Liu C. Decellularized extracellular matrix scaffolds: Recent trends and emerging strategies in tissue engineering. *Bioact Mater*. 2022; 10:15-31. doi: j.bioactmat.2021.09.014
17. Lu J, Huang J, Jin J, Xie C, Xue B, Lai J. The design and characterization of a strong Bio-Ink for meniscus regeneration. *IJB*. 2022;8(4):600. doi: 10.18063/ijb.v8i4.600
18. Nerger BA, Sinha S, Lee NN, *et al*. 3D hydrogel encapsulation regulates nephrogenesis in kidney organoids. *Adv Mater*. 2024;36(14):2308325. doi: 10.1002/adma.202308325
19. Lee J, Hong J, Kim W, Kim GH. Bone-derived dECM/alginate bioink for fabricating a 3D cell-laden mesh structure for bone tissue engineering. *Carbohydr Polym*. 2020;250:116914. doi: j.carbpol.2020.116914

20. Rizzo R, Ruetsche D, Liu H, Zenobi-Wong M. Optimized photoclick (bio)resins for fast volumetric bioprinting. *Adv Mater*. 2021;33(49):2102900. doi: 10.1002/adma.202102900

21. Chen S, Wu C, Zhou T, *et al*. Aldehyde-methacrylate-hyaluronan profited hydrogel system integrating aligned and viscoelastic cues for neurogenesis. *Carbohydr Polym*. 2022;278:118961. doi: 10.1016/j.carbpol.2021.118961

22. Milton LA, Davern JW, Hipwood L, *et al*. Liver click dECM hydrogels for engineering hepatic microenvironments. *Acta Biomater*. 2024;185:144-160. doi: 10.1016/j.actbio.2024.06.037

23. Elvitigala KCML, Mohan L, Mubarok W, Sakai S. Phototuning of hyaluronic-acid-based hydrogel properties to control network formation in human vascular endothelial cells. *Adv Healthc Mater*. 2024;13(17):2303787. doi: 10.1002/adhm.202303787

24. Lim KS, Schon BS, Mekhileri NV, *et al*. New visible-light photoinitiating system for improved print fidelity in gelatin-based bioinks. *ACS Biomater Sci Eng*. 2016;2(10):1752-1762. doi: 10.1021/acsbiomaterials.6b00149

25. Kim H, Kang B, Cui X, *et al*. Light-activated decellularized extracellular matrix-based bioinks for volumetric tissue analogs at the centimeter scale. *Adv Funct Mater*. 2021;31(32):2011252. doi: 10.1002/adfm.202011252

26. Wang L, Riediger L, Rao Q, *et al*. Tunable synthetic hydrogel modulates hepatic lineage specification of human liver organoid. *Adv Funct Mater*. 2025;19(8):e08430. doi: 10.1002/adfm.202508430

27. Fang W, Yang M, Wang L, *et al*. Hydrogels for 3D bioprinting in tissue engineering and regenerative medicine: current progress and challenges. *IJB*. 2023;9(5):759. doi: 10.18063/ijb.759

28. Wang Z, Boretto M, Millen R, *et al*. Rapid tissue prototyping with micro-organospheres. *Stem Cell Rep*. 2022;17(9):1959-1975. doi: 10.1016/j.stemcr.2022.07.016

29. Liu F, Liu C, Chen Q, *et al*. Progress in organ 3D bioprinting. *IJB*. 2024;4(1):128. doi: 10.18063/ijb.v4i1.128

30. Hu Y, Zhu T, Cui H, Cui H. Integrating 3D bioprinting and organoids to better recapitulate the complexity of cellular microenvironments for tissue engineering. *Adv Healthc Mater*. 2024;14(3):2403762. doi: 10.1002/adhm.202403762

31. Choi Y mi, Lee H, Ann M, Song M, Rheey J, Jang J. 3D bioprinted vascularized lung cancer organoid models with underlying disease capable of more precise drug evaluation. *Biofabrication*. 2023;15(3):034104. doi: 10.1088/1758-5090/acd95f

32. Han Y, Yang J, Zhao W, *et al*. Biomimetic injectable hydrogel microspheres with enhanced lubrication and controllable drug release for the treatment of osteoarthritis. *Bioact. Mater*. 2021;6(10):3596-3607. doi: 10.1016/j.bioactmat.2021.03.022

33. Rawal P, Tripathi DM, Ramakrishna S, Kaur S. Prospects for 3D bioprinting of organoids. *Bio-Des Manuf*. 2021;4(3):627-640. doi: 10.1007/s42242-020-00124-1

34. Alam K, Nair L, Mukherjee S, *et al*. Cellular interplay to 3D in vitro microphysiological disease model: cell patterning microbiota–gut–brain axis. *Bio-Des Manuf*. 2024;7(3):320-357. doi: 10.1007/s42242-024-00282-6

35. Keselowsky BG, Bridges AW, Burns KL, *et al*. Role of plasma fibronectin in the foreign body response to biomaterials. *Biomaterials*. 2007;28(25):3626-3631. doi: j.biomaterials.2007.04.035

36. Xie M, Lian L, Mu X, *et al*. Volumetric additive manufacturing of pristine silk-based (bio)inks. *Nat Commun*. 2023;14(1):210. doi: 10.1038/s41467-023-35807-7

37. Yang H, Zeng T, Jiang T, *et al*. Recent progress on functional hydrogels as biomaterial for biomedicine. *Results Chem*. 2025;16:102464. doi: 10.1016/j.rechem.2025.102464

38. Datta P, Barui A, Wu Y, Ozbolat V, Moncal KK, Ozbolat IT. Essential steps in bioprinting: from pre- to post-bioprinting. *Biotechnol Adv*. 2018;36(5):1481-1504. doi: 10.1016/j.biotechadv.2018.06.003

39. Luo Y, He X, Du Q, *et al*. Metal-based smart nanosystems in cancer immunotherapy. *Exploration*. 2024;4(6):20230134. doi: 10.1002/EXP.20230134

40. Chen B, Guo K, Zhao X, *et al*. Tumor microenvironment-responsive delivery nanosystems reverse immunosuppression for enhanced CO gas/immunotherapy. *Exploration*. 2023;3(6):20220140. doi: 10.1002/EXP.20220140